Multiscale identification of local tetragonal distortion in $NaNbO_3$-$BaTiO_3$ weak relaxor ferroelectrics by Raman, synchrotron x-ray diffraction, and absorption spectra

Ruzhong Zuo,[1,a)] He Qi,[1] Jian Fu,[1] Jing-Feng Li,[2] and Longtu Li[2]
[1]*Institute of Electro Ceramics and Devices, School of Materials Science and Engineering, Hefei University of Technology, Hefei 230009, People's Republic of China*
[2]*State Key Laboratory of New Ceramics and Fine Processing, School of Materials Science and Engineering, Tsinghua University, Beijing 100084, People's Republic of China*

(Received 10 July 2017; accepted 15 September 2017; published online 26 September 2017)

Locally persistent tetragonal distortion in $NaNbO_3$-$BaTiO_3$ relaxor ferroelectrics was identified at multiple length scales by means of *in-situ* synchrotron x-ray diffraction, absorption fine structure, and Raman spectra although their average symmetry seemingly evolved from a tetragonal to a cubic-like phase with the increasing $BaTiO_3$ content. Theoretical calculations of Nb-O peaks in the *R* range of 1–2 Å provided a clear evidence that Nb^{5+} in an NbO_6 octahedron should be spontaneously shifted along [001]. The competition between B-site Nb^{5+} ([001]) and Ti^{4+} ([111]) spontaneous off-center displacement directions would contribute to the disruption of long-range polar ordering. Raman spectra suggested that A-site Ba^{2+} and Na^{+} cations should be located at the center of the cubes in the absence of the polar contribution unlike Pb^{2+}/Bi^{3+} with lone-pairs. A relatively low field-induced strain in NN-BT relaxors was thus ascribed to the small spontaneous polarization magnitude and the absence of structural phase transition during electric loading. *Published by AIP Publishing.*
[http://dx.doi.org/10.1063/1.4995009]

Perovskite-structured piezoelectrics such as $Pb(Zr,Ti)O_3$ (PZT) are usually chemically designed in the proximity of a morphotropic phase boundary (MPB) between rhombohedral (R) and tetragonal (T) phases, in which enhanced piezoelectric properties can be attained owing to the increased number of spontaneous polarization (P_s) directions. Different from normal MPB compositions, another type of MPB composition can be formed in perovskite solid solutions between ferroelectrics and relaxors with increasing the relaxor fraction, accompanying a composition induced T-R (or pseudocubic, PC) phase structural transition.[1,2] Moreover, the origin of ferroelectricity in perovskites is believed to arise from the off-center displacement of B-site cations (Nb^{5+}, Ti^{4+}, etc.) within the BO_6 octahedron. This distortion is usually driven by the hybridization of the empty d-orbitals of B-site ions with the O p-orbitals.[3] As long-range ferroelectric ordering was disrupted into polar nanoregions (PNRs), the materials would macroscopically exhibit a broad and frequency-dependent dielectric permittivity peak. This is generally attributed to the formation of local random fields, which would determine the size and dynamics of PNRs.[4] The application of external electric fields was found to play an extremely different role in stabilizing PNRs. An irreversible phase transition from nonergodic relaxors to normal ferroelectric states can be electrically driven, while the field induced transition from ergodic relaxor to long-range ferroelectric order proved to be completely reversible. This reversible process generated significantly enhanced strains of ~0.3%–0.5% in a couple of relaxor ferroelectric ceramics such as La-PZT, $BiFeO_3$, and $(Bi_{0.5}Na_{0.5})TiO_3$ (BNT)-based compositions.[5–7] Bi^{3+} and Pb^{2+} have a similar $6s^2$ lone-pair electron configuration,[8,9] which would induce strong hybridization with oxygen. The *in-situ* Raman study indicated that the loss of the macroscopic ferroelectricity in the relaxor zone of BNT-based ceramics should be related to the loss of hybridization between the Bi^{3+} $6s^2$ orbitals and the oxygen 2p orbitals.[10] We wonder how perovskite-type relaxor ferroelectrics without lone pairs would behave in terms of their macroscopic symmetry, local structure, and strains.

$NaNbO_3$ (NN)-based relaxor ferroelectrics have attracted much attention in recent years as a lead-free candidate material system.[11–14] Among them, $(1-x)$NN-$x$$BaTiO_3$ ($(1-x)$NN-xBT) solid solutions belonged to a lone-pair-free material system and were reported to undergo a successive phase transition.[15] In this communication, a weak relaxor behavior of $(1-x)$NN-xBT ceramics with $x = 0.15$–0.25 was investigated with a corresponding change of the average phase structure from T to PC. Accompanied by the loss of macroscopic symmetry, a local T distortion was at multiple length scales identified even in samples with $x \geq 0.22$ by means of synchrotron x-ray diffraction (XRD), extended x-ray absorption fine structure (EXAFS), and Raman spectra. These results facilitated us to attain a good understanding of the underlying mechanism for the evolution of piezoelectric properties and strains in NN-BT lead-free ceramics.

$(1-x)$NN-xBT ceramics were prepared via a solid-state reaction method. The detailed experimental procedure could be referred elsewhere.[16] A conventional XRD was measured at room temperature (RT) by using a powder X-ray diffractometer (D/MAX-RB, Rigaku, Tokyo, Japan) using Cu $K\alpha$ radiation. Dielectric properties as a function of temperature and frequency were measured by using an LCR meter (Agilent E4980A, Santa Clara, CA). The ferroelectric testing system (Precision Multiferroic, Radiant Technologies Inc.,

a)Author to whom correspondence should be addressed: rzzuo@hotmail.com. Tel.: 0086-551-62905285. Fax: 0086-551-62905285.

Albuquerque, NM) connected with a laser interferometric vibrometer (SP-S 120, SIOS Meβtechnik GmbH, Germany) was used to measure polarization versus electric field (P-E) hysteresis loops and strain versus electric field (S-E) curves at 10 Hz. *In-situ* XRD measurements on gold sputtered disks were taken at beam line 14B1 ($\lambda = 1.2378$ Å) at Shanghai Synchrotron Radiation Facility (SSRF) in a symmetric reflection geometry.[17] Raman spectra were collected on well-polished pellets using 532-nm excitation at RT using a Raman spectrometer (LabRam HR Evolution, HORIBA JOBIN YVON, Longjumeau Cedex, France). The EXAFS spectrum of the Nb K-edge was recorded in the transmission mode at beam line 01C1 of National Synchrotron Radiation Research Center (NSRRC, Hsinchu, Taiwan) by using a Si(111) double-crystal monochromator and then analyzed with IFEFFIT package.[18]

The dielectric permittivity versus frequency and temperature curves are locally shown in Fig. 1(a) for the $x = 0.15$ and $x = 0.22$ ceramics (similar curves for all studied samples in a wide temperature range can be seen in Fig. S1, supplementary material). The dielectric peak became more diffuse and more dependent on measuring frequency with increasing x, in addition to a gradually declined temperature (T_m) at the dielectric maxima, indicating a typical relaxor ferroelectric as $x \geq 0.15$. The $x = 0.1$ sample was reported to be a normal T ferroelectric phase at RT.[15] This means that the addition of BT into NN induced a normal to relaxor ferroelectric phase transition. The empirical *Vogel-Fulcher* law was used to determine the freezing temperature T_f in a canonical relaxor.[19] A T_f value of ~23 °C at $x = 0.22$ indicates that the composition was located at the boundary between ergodic and nonergodic relaxor states, as shown in Fig. 1(b) where a pinched P-E loop together with a current density versus electric field (J-E) curve with four polarization current peaks was observed during one electric cycle. As expected, the unipolar strain (S_u) reached the maximum value of ~0.17% at 6 kV/mm as $x = 0.22$ owing to a field induced reversible relaxor to ferroelectric phase transition, as shown in Fig. 1(c). The evolution of dielectric relaxation behavior with x was also manifested by the change of average phase structures [Fig. 1(d)]. According to the average phase structure change, there seemingly exists a phase boundary between T and PC phases in the proximity of $x = 0.21$, however, near which quasi-static piezoelectric constant d_{33} values were not maximized. In many solid solution systems, a normal to relaxor ferroelectric phase transition accompanied a phase structural transition from T/R to R/PC phases, during which an MPB formed. Moreover, it is known that one of the most important structural characteristics for relaxors should be the existence of the PNRs, which are small spontaneously polarized clusters in the non-polar matrix. Therefore, it is essential to find out what the intrinsic symmetry of PNRs or the local lattice distortion would be particularly as $x \geq 0.22$.

Figures 2(a)–2(h) show *in-situ* synchrotron XRD results of the $x = 0.22$ sample at RT. In accordance with conventional XRD results, it looked like a PC symmetry at zero field (also see Fig. S2, supplementary material). As a small field of 0.2 kV/mm was applied, a split (200) diffraction peak started to be resolved. Meanwhile, the intensity ratio of (002)/(200) peaks gradually increased from ~0.13 to ~0.33 as the electric field rose from 0.2 kV/mm to 0.8 kV/mm [Fig. 2(i)]. The (002)/(200) peak intensity ratio at 0.8 kV/mm just approximated to the structural factor (1/3) of a normal T phase, meaning that PNRs have evolved into ferroelectric microdomains. This is because the application of a small field could suppress the energy fluctuation of the system. More PNRs could stably appear, such that the size of PNRs exceeded the coherence length to be detected by an XRD. These weakly correlated PNRs evolved into microdomains by merging small ones at 0.8 kV/mm. These results provided a direct proof that the local T symmetry on nanoscale was not broken although the macroscopic symmetry looked cubic. A continuous increase in the (002)/(200) intensity ratio with fields suggests an obvious domain switching along

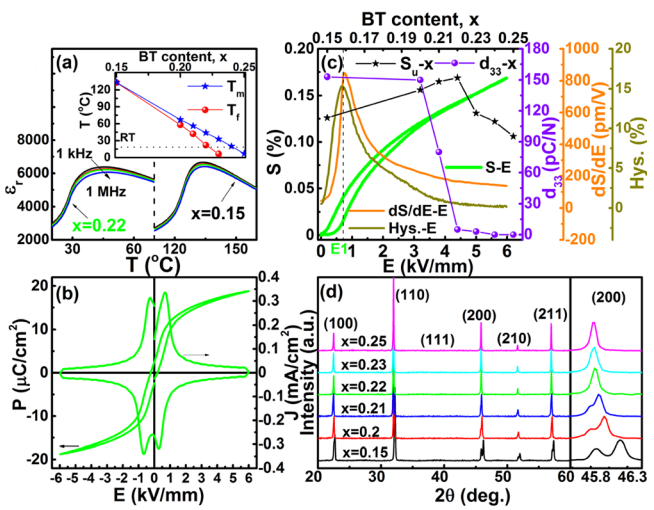

FIG. 1. (a) Temperature and frequency dependent dielectric permittivity of the virgin $x = 0.15$ and $x = 0.22$ ceramics; the inset in (a) shows the variation of T_m and T_f values with changing x, (b) P-E loop and the corresponding J-E curve at 10 Hz measured at RT for the $x = 0.22$ ceramic, (c) the unipolar S-E curves at 10 Hz and the electric field dependent dS/dE values and strain hysteresis of the $x = 0.22$ ceramic, as well as the quasi-static d_{33} and the unipolar strain S_u at 6 kV/mm varying with x, and (d) XRD patterns of (1-x)NN-xBT ceramics as indicated.

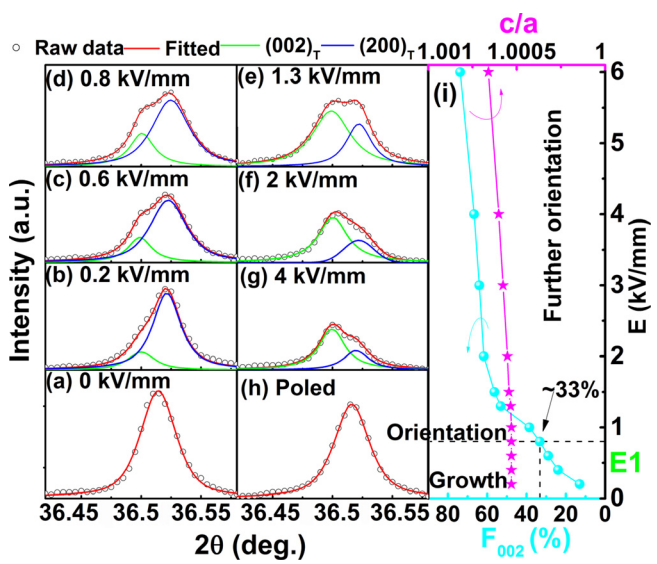

FIG. 2. (a)–(h) The (200) reflections of the $x = 0.22$ ceramic under *in-situ*/*ex-situ* electric fields shown representatively and fitted by using PeakFit software as indicated, and (i) electric field dependent F_{002} and c/a values for the $x = 0.22$ ceramic.

the *c*-axis, as clearly seen from the calculated domain texture F_{002} [see Fig. 2(i)].[20] Nevertheless, a T symmetry was maintained up to a field of 6 kV/mm. Also, the *c*/*a* value remained almost constant with electric fields [Fig. 2(i)], indicating that the unit cell polarity was not altered by external fields. By comparison, an obvious domain switching and even ferroelectric phase transition can be observed in normal ferroelectrics. If one carefully looked at the evolution of the strain hysteresis (Hys.) and the change velocity of strain with fields (dS/dE) in Fig. 1(c), both peak values of Hys. and dS/dE appeared at a similar electric field E1 of 0.8 kV/mm. This suggests that the electric field forced PNR growth process dominated the fastest increase of field induced strains and the formation of the maximum strain hysteresis,[21] instead of the subsequent domain switching. As shown in Fig. 2(h), all reflections were completely recovered as the applied electric field was released, indicating that the process of field forced PNR growth and domain switching was reversible. This conformed to the nature of ergodicity of the $x = 0.22$ sample.

It is known that the analysis of the wavenumber, intensity, and/or line width evolution of the Raman spectra for different samples was expected to give insight into the change in local structure evolution, as shown in Figs. 3 and S3 (supplementary material). The Raman spectrum for the $x = 0.1$ sample is included for comparison. These results provide sufficient evidence that on a smaller length-scale, the symmetry of all compositions, particularly for $x \geq 0.22$, should be different from the cubic $Pm\bar{3}m$, in which all atoms are located in sites having a center of inversion and therefore no first-order Raman scattering is allowed. In the low wavenumber region, e.g., $<150\,cm^{-1}$, the modes are associated with the vibration of A-site ions, such as Ba^{2+} and Na^{+}.[22,23] Two distinct modes at $47\,cm^{-1}$ and $85\,cm^{-1}$ showed little frequency shift with increasing *x* [see Fig. 3(a)], indicating that there was no orbital hybridization between A-site cations and oxygen. This is related to the ionic character of the Na/Ba-O bonds. It suggests that Na^{+} and Ba^{2+} cations should remain in the center of the O_{12} cages. By comparison, both $\nu1$ and $\nu5$ modes showed an evident shift to low wavenumbers with increasing *x*, indicating that the Nb/Ti-O vibrations became softened gradually, which is due to the weakening of the bonding between B-site cations and oxygen.

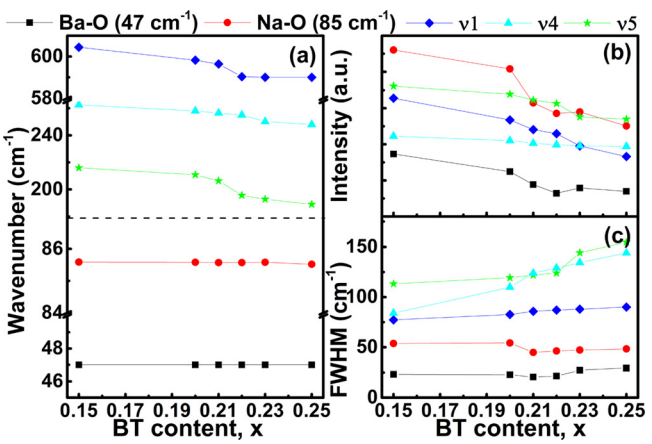

FIG. 3. The composition dependence of (a) wavenumber, (b) peak intensity, and (c) FWHM for several selected Raman modes as indicated.

The weakening of the B-O bonds is compatible with the appearance of the macroscopic relaxor behavior since the loss of hybridization between the empty Nb^{5+}/Ti^{4+} d-orbitals and the oxygen p-orbitals is closely related to the dynamics of the PNRs.[24] A steady phonon softening, an evident increase of FWHM, and an obvious decrease of the peak intensity for $\nu1$ and $\nu5$ modes should correspond to the increase of the structural disorder and the decrease of the unit cell polarity, as shown in Figs. 3(b) and 3(c). This was in agreement with the declined *c*/*a* value observed in Fig. 1(d). It is noteworthy that the splitting of the Ti/Nb-O modes ($\nu5$ and $\nu4$) was preserved in all studied compositions, suggesting the T character of the unit cell.[10] This is because the A1 mode ($\nu4$) represents the double-degenerate O-B-O stretching vibration in which oxygen is situated along the *c*-axis; however, the E mode ($\nu5$) corresponds to the triple-degenerate O-B-O bending vibration where the oxygen is located at the ab plane perpendicular to the c-axis.

To further investigate the effect of B-site cations on the local structure and polarization, the Fourier transform (FT) magnitudes of the k^3 weighted Nb *K*-edge x-ray absorption fine structure (XAFS) spectra of $(1-x)$NN-*x*BT samples are shown in Fig. 4. The FTs of all samples can be readily separated into three contributions including BO_6 octahedra and isolated A-site ions in the *R* range of 1–4 Å. The terms *R* represents the distance from the neighboring atom to the absorption atom. The first oxygen shell was found to be nearly identical, as clearly seen from the FT peaks in the *R* range of 1–2 Å. This suggests that the first-neighbor's environment around Nb atoms was very close. The change of the nearest Nb coordinated shell around the absorption Nb atoms can be disclosed by the FT peak in the *R* range of 3–4 Å, in which the asymmetric peaks of the FTs in all samples indicated the existence of the local lattice distortion. The decline of the peak asymmetry further meant a weakening lattice distortion.

The peak fitting of the FTs was carried out in the *R* range of 1–2 Å and 3–4 Å, as shown in Figs. S4 and S5 (supplementary material), respectively. In the oxygen shell, all fits were attempted using T-distorted NbO_6 octahedra, which contain three different Nb-O distances: Nb-O21 (path 1),

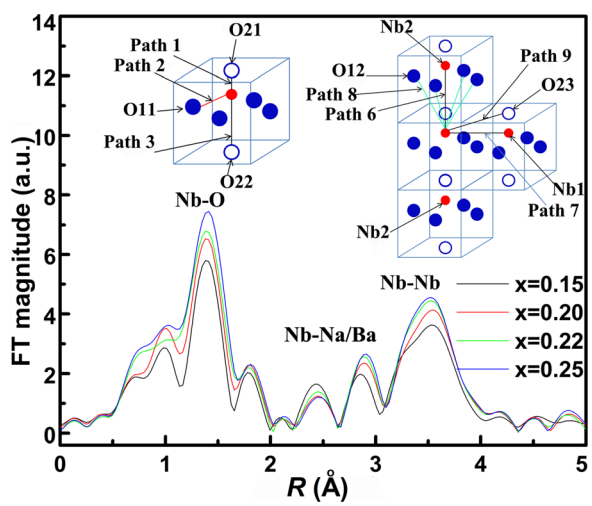

FIG. 4. Fourier transforms of the k^3-weighted Nb *K*-edge EXAFS spectra of (1-*x*)NN-*x*BT samples at RT; the inset shows the sketch of selected scattering paths in the *R* range of 1–2 Å and 3–4 Å, respectively.

Nb-O22 (path 3), and Nb-O11 (path 2) as shown in the inset of Fig. 4. By comparison, the peak fitting in the R range of 3–4 Å was more complicated. In this R range, the peaks of FTs are usually dominated by the nearest Nb atoms (paths 6 and 7). However, FT components of the bonds between Nb atoms and 4 equatorial O1 atoms in the neighboring octahedron (path 8) and the bonds between Nb atoms and 4 O2 atoms in the neighboring octahedron along the c axis (path 9) should also appear. Here, the Debye-Waller factor $\sigma^2_{\text{Nb-O12}} = \sigma^2_{\text{Nb-O23}}$ was assumed to decrease the number of the independent variables for the fitting. The structure parameters obtained from the fitting are shown in Table S1 (supplementary material). These results indicate that each fitted profile agreed reasonably with the experimental FT profile, clearly confirming a local T distortion in the $x = 0.22$ sample as we used it as a structure model.

The Nb off-center displacement was evaluated to be ~0.16 Å using $R_{\text{Nb-O22}} - R_{\text{Nb-Nb2}}/2$ as listed in Table S1 (supplementary material), being independent of the Ti content. A similar phenomenon was observed in BT-$BaZrO_3$ (BZT) with an identical Ti displacement of ~0.18 Å, although Zr is not ferroelectrically active.[25] The direction of the Nb displacement could be further identified by means of theoretical calculations of Nb-O peaks for an NbO_6 octahedron, in which we used an NbO_6 octahedron with Nb displacement along [001] and [111] directions. At the same time, A-site atoms and oxygen atoms were assumed to be at the corners of the cube and the center of the face diagonal without any off-center shift, respectively. As shown in Fig. 5, a double-peak structure for the Nb-O peak was observed in the R range of 1–2 Å. The Nb-O peak in the calculations with [001] Nb displacement looked very similar to that of the experimental data for the $x = 0.22$ sample, suggesting that the Nb off-center displacement in this sample is mainly along the [001] direction. It is reasonable to believe that the spontaneous displacement of Ti ions in NN-BT should be along [111], although the Ti XAFS spectra were not measured in the current study. This is because a [111] Ti spontaneous displacement usually occurred in BZT and other BT based relaxors, irrespective of their average phase structures, such as T, O, or R.[26,27] As a result, the interference between two different spontaneous displacement directions of Nb ([001]) and Ti ([111]) cations would help destroy the long-range polar correlation, although B-sites in NN-BT were occupied by two ferroelectric-active cations. A similar phenomenon was also observed in typical relaxor ferroelectric PMN, where Pb atoms are locally shifted along [001] directions while Mg/Nb atoms are locally shifted along [111] directions.[28] Moreover, the above Raman results proved that A-site Na and Ba cations should lie at the corners of the cube without any off-center shift. By comparison, a local off-center displacement of Pb and Bi cations as large as ~0.3–0.5 Å was achieved in typical Pb/Bi-based relaxor ferroelectrics due to the lone-pair electron effect.[29–31] As a result, a weak P_s due to absence of the hybridization of A-site ions and oxygen, as well as no structural phase transition involved in during electric loading (Fig. 2), would lead to a relatively low electrostrain value in NN-BT relaxor ferroelectrics (Fig. 1).

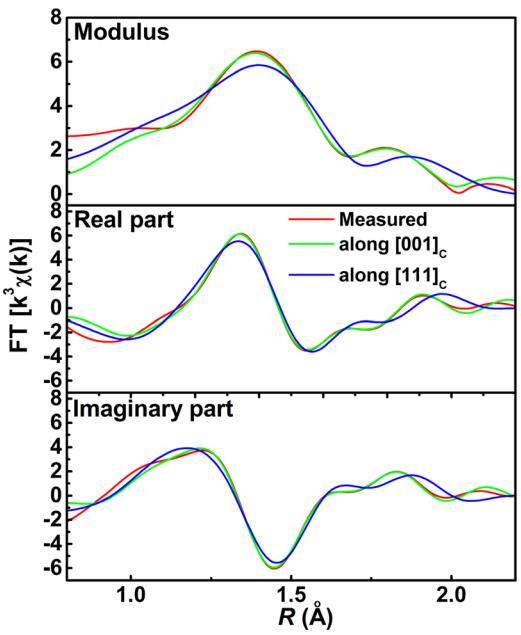

FIG. 5. The Nb K-edge R space data of the $x = 0.22$ sample and the calculations with Nb off-center displacements along [001] and [111] directions.

In summary, the substitution of BT for NN was found to induce a transition from a normal to relaxor ferroelectric in a lead-free NN-BT binary system, corresponding to an average phase structural transition from T to PC. *In-situ* synchrotron XRD, Nb K-edge EXAFS spectra, and Raman spectra strongly suggested that a local T lattice distortion should be maintained, irrespective of the BT content in the studied composition range. The competition between different local displacement directions of B-site Nb ([001]) and Ti ([111]) would tend to disrupt the long-range ferroelectric ordered state. The low P_s owing to the lack of A-site polar contributions and the absence of structural phase transition during electric loading should be responsible for relatively small field induced strains in the NN-BT system.

See supplementary material for the temperature dependent dielectric permittivity curves, *in-situ* synchrotron XRD results, composition dependent Raman spectra, and FT magnitudes of Nb K-edge EXAFS spectra and the fitting results.

This work was supported by the National Natural Science Foundation of China (Grant Nos. U1432113, 51402079, and 51332002).

[1]N. Vittayakorn, G. Rujijanagul, X. Tan, M. A. Marquardt, and D. P. Cann, J. Appl. Phys. **96**, 5103 (2004).
[2]A. K. Singh, D. Pandey, and O. Zaharko, Phys. Rev. B **74**, 024101 (2006).
[3]R. E. Cohen, Nature **358**, 136 (1992).
[4]B. E. Vugmeister, Phys. Rev. B **73**, 174117 (2006).
[5]X. H. Dai, Z. Xu, J. F. Li, and D. Viehland, J. Appl. Phys. **79**, 2023 (1996).
[6]L. L. Fan, J. Chen, S. Li, H. J. Kang, L. J. Liu, L. Fang, and X. R. Xing, Appl. Phys. Lett. **102**, 022905 (2013).
[7]H. Simons, J. E. Daniels, J. Glaum, A. J. Studer, J. L. Jones, and M. Hoffman, Appl. Phys. Lett. **102**, 062902 (2013).
[8]P. S. Halasyamani, Chem. Mater. **16**, 3586 (2004).
[9]A. Walsh, D. J. Payne, R. G. Egdell, and G. W. Watson, Chem. Soc. Rev. **40**, 4455 (2011).
[10]D. Schütz, M. Deluca, W. Krauss, A. Feteira, T. Jackson, and K. Reichmann, Adv. Funct. Mater. **22**, 2285 (2012).

[11]A. Aydi, S. Chkoundali, H. Khemakhem, A. Simon, and R. Von Der Mühll, J. Alloys Compd. **465**, 222 (2008).
[12]I. P. Raevski and S. A. Prosandeev, J. Phys. Chem. Solids **63**, 1939 (2002).
[13]A. Aydi, H. Khemakhem, C. Boudaya, R. Von der Mühll, and A. Simon, Solid State Sci. **6**, 333 (2004).
[14]R. Z. Zuo, H. Qi, and J. Fu, Appl. Phys. Lett. **109**, 022902 (2016).
[15]J. T. Zeng, K. W. Kwok, and H. L. W. Chan, J. Am. Ceram. Soc. **89**, 2828 (2006).
[16]R. Z. Zuo, H. Qi, J. Fu, J. F. Li, M. Shi, and Y. D. Xu, Appl. Phys. Lett. **108**, 232904 (2016).
[17]T. Y. Yang, W. Wen, G. Z. Yin, X. L. Li, M. Gao, Y. L. Gu, L. Li, Y. Liu, H. Lin, X. M. Zhang, B. Zhao, T. K. Liu, Y. G. Yang, Z. Li, X. T. Zhou, and X. Y. Gao, Nucl. Sci. Tech. **26**, 020101 (2015).
[18]B. Ravel and M. Newville, J. Synchrotron Radiat. **12**, 537 (2005).
[19]A. K. Tagantsev, Phys. Rev. Lett. **72**, 1100 (1994).
[20]J. Fu, R. Z. Zuo, Y. D. Xu, J. F. Li, and M. Shi, J. Eur. Ceram. Soc. **37**, 975 (2017).
[21]R. Z. Zuo, F. Li, J. Fu, D. G. Zheng, W. L. Zhao, and H. Qi, J. Eur. Ceram. Soc. **36**, 515 (2016).
[22]G. Burns, Phys. Rev B **10**, 1951 (1974).
[23]Z. X. Shen, X. B. Wang, M. H. Kuok, and S. H. Tang, J. Raman Spectrosc. **29**, 379 (1998).
[24]V. R. Mastelaro, H. R. Favarim, A. Mesquita, A. Michalowicz, J. Moscovici, and J. A. Eiras, Acta Mater. **84**, 164 (2015).
[25]C. Laulhe, F. Hippert, R. Bellissent, A. Simon, and G. J. Cuello, Phys. Rev. B **79**, 064104 (2009).
[26]B. Ravel, E. A. Stern, R. I. Vedrinskii, and V. Kraizman, Ferroelectrics **206**, 407 (1998).
[27]E. A. Stern, Phys. Rev. Lett. **93**, 037601 (2004).
[28]I. K. Jeong, T. W. Darling, J. K. Lee, T. Proffen, R. H. Heffner, J. S. Park, K. S. Hong, W. Dmowski, and T. Egami, Phys. Rev. Lett. **94**, 147602 (2005).
[29]I. Grinberg and A. M. Rappe, Phys. Rev. B **70**, 220101(R) (2004).
[30]I. Grinberg, M. R. Suchomel, W. Dmowski, S. E. Mason, H. Wu, P. K. Davies, and A. M. Rappe, Phys. Rev. Lett. **98**, 107601 (2007).
[31]V. A. Shuvaeva, D. Zekria, A. M. Glazer, Q. Jiang, S. M. Weber, P. Bhattacharya, and P. A. Thomas, Phys. Rev. B **71**, 174114 (2005).